

# **Response Comparison for the Hybrid III, THOR Mod Kit with SD-3 Shoulder, and PMHS in a Simulated Frontal Crash**

**Greg Shaw**

**David Lessley**

**Joe Ash**

**Jeff Crandall**

University of Virginia

Center for Applied Biomechanics

United States

**Dan Parent**

Human Injury Research Division

NHTSA

**Paper Number 13-0130**

## **ABSTRACT**

This study evaluated the kinematic and chest deflection responses of a THOR Mod Kit dummy with the Chalmers/Humanetics SD-3 shoulder and the 50<sup>th</sup> percentile Hybrid III (H3) in the frontal impact 40 km/h 14 g Gold Standard 1 (GS1) test condition. THOR and H3 biofidelity were evaluated by comparing dummy response to the response of 8 post mortem human surrogates (PMHS) in prior GS1 tests. The subject was restrained by a three-point lap and shoulder belt in a right-front passenger configuration. Pelvis and lower extremity movements were restricted using a rigid knee bolster and footrest which were adjusted to be in contact with the knees and feet of each subject at the time of impact.

The THOR SD-3 shoulder sustained no damage during the course of the nine test series. In general, THOR peak x-axis chest deflection values for the anterior measurement sites were closer to those of the PMHS than the H3. However, the deflection response of neither dummy approached that of the PMHS relative to the motion of the anterior ribcage away from the spine. The THOR SD-3 exhibited a PMHS-like deflection sensitivity to belt position, a characteristic reported for the H3 (Horsch et al 1991).

The PMHS rearward motion of the loaded shoulder may result in increased chest deflection, while the forward motion of the THOR SD-3 may limit chest deflection. The H3 loaded shoulder motion was likely limited by the stiff H3 shoulder design and lack of range of motion. Because the shoulder interaction with the belt is a determinant of chest deflection, further study of the THOR SD-3 shoulder belt interaction is suggested. Similarly a comprehensive study of spinal kinematics with focus on spinal rotations that may substantially influence interaction between the ribcage and the shoulder belt is also warranted.

## **INTRODUCTION**

While increased seat belt usage and advances in restraint design have, on average, substantially improved the injury outcome for restrained occupants, numerous fatalities and debilitating injuries are still occurring nonetheless (Viano and Ridella 1996, Elvik and Vaa 2004, NHTSA 2008, NHTSA 2009). For restrained vehicle occupants, injuries to the head and thorax are primary sources of mortality occurring from motor vehicle accidents (Huelke et al 1979, Backaitis and Dalmotas 1985, Viano et al 1986, Foret-Bruno et al 1994, Allsop and Kennett 2002, Morris et al 2002, Morris et al 2003, Kent et al 2007). This is especially true for older

occupants who are more susceptible to injury resulting from the restraining forces applied to the torso during a crash (Morris et al 2002, Morris et al 2003, Kent et al 2007). The combination of societal aging and the associated vulnerability of older persons to restraint loading injuries is a principal motivation for continued passenger safety research (Rouhana et al 2003, Bostrom and Haland 2003, Forman et al 2006). Further mitigating injuries to restrained occupants requires a more complete understanding of how the human skeletal system moves during a crash event. Occupant kinematics not only dictate the potential for contact between the vulnerable head and the interior structures of the vehicle, but also determines the interaction between the restraint system and the thorax.

Effectively evaluating the performance of current restraint systems, as well as optimizing future restraint designs, requires the use of biofidelic evaluation tools to emulate human occupant motion and to predict injury during an impact event. Anthropomorphic testing devices (ATDs) and computational models are the most commonly utilized human surrogates for this purpose.

Improved biofidelity of ATD motion and the response of the chest subjected to restraint loading remains a priority for improving frontal impact dummies. A simulated impact (sled test) provides the most realistic conditions for defining human response, as approximated by post mortem human surrogates (PMHS) and subsequently for assessing dummy biofidelity. A frontal sled test involves restraint loading of both the chest and the shoulder complex, a structure that can affect the amount of normal shoulder belt loading applied to the anterior chest.

In support of the National Highway Traffic Safety Administration (NHTSA) effort to enhance the biofidelity of the Test Device for Human Occupant Restraint (THOR) (Ridella and Parent 2011), this study evaluated the kinematic and chest deflection responses of a THOR Mod Kit dummy (SN 16) with the Chalmers/Humanetics SD-3 shoulder (THOR SD-3, for short) (Figure 1) and the 50<sup>th</sup> percentile Hybrid III (H3) in the frontal impact 40 km/h 14 g Gold Standard 1 (GS1) test condition, described in detail by Shaw et al 2009 (Figure 2). The THOR SD-3 was fitted with a shoulder designed to be more humanlike in both geometry and motion in comparison to that of the original THOR shoulder (Lemmen et al 2013). THOR SD-3 and H3 biofidelity was evaluated by comparing dummy response to the response of 8 PMHS in prior GS1 tests (Table 1) (Shaw et al 2009).

**Table 1: Test Matrix**

Test Condition		# of tests		
		H3	THOR SD-3	PMHS
<b>GS1</b>	<b>Gold Standard Condition 1 40km/h, Standard Belt</b>	3	3	8

## METHODOLOGY

The subject was forward-facing and restrained in a right-front passenger configuration. Subject and restraint positioning were tightly controlled to reduce test-to-test variability. The test fixture (Figure 3) and test methodology, described by Shaw et al 2009, was designed to provide a reasonable approximation of a real-world frontal crash with a restrained occupant while providing repeatable and reproducible test conditions that would allow whole-body kinematic response to be comprehensively measured and analyzed. The restraint consisted of a 3-point lap and shoulder belt with anchor positions approximating those found in a typical mid-size U.S. sedan. The belt did not include a retractor and did not allow for pass-through at the representation of the buckle. The webbing material, which was replaced for each test, was manufactured by Narricut (International twill pattern 13195, 6-8% elongation). Pelvis and lower extremity movements were restricted

using a rigid knee bolster and footrest which were adjusted to be in contact with the knees and feet of each subject at the time of impact. The combination of lap belt, knee bolster, and footrest was designed to minimize pelvic and lower extremity movements during the impact event while allowing the characteristic forward torso motion associated with an actual automotive restraint system.

### **SD-3 Shoulder Durability Monitoring**

In previous testing with the Chalmers SD1 shoulder (Shaw et al 2010), mechanical failure occurred in the joint connecting the upper arm to the shoulder after three tests were carried out. Similar issues were discovered in testing with the SD-2 shoulder, though the number of tests that were carried out before mechanical failure occurred is not clear. Thus, the durability of the SD-3 shoulder was carefully monitored during this test series that included the three tests reported in this paper and an additional six tests with a force-limited shoulder belt. With the jacket removed, the shoulder was examined and manipulated before the test series and after each of the tests with special attention to the distal clavicle ball joint, polymer bumper stops, and fastener security.

### **Subject Kinematics**

A 16-camera, 1000 Hz optoelectronic stereophotogrammetric system (Vicon, MX series, Oxford, UK) was used to obtain trajectories of retroreflective target clusters (Figure 4) attached to the head, spine, shoulders, and pelvis of each subject. The recorded trajectories of the attached target clusters were used to calculate the trajectories of selected underlying anatomical structures using a coordinate transformation and the assumption of rigid body motion described in detail by (Lessley et al. 2011). Using the methodology described by Parent et al, 2012, kinematics were calculated at consistent anatomical landmarks for both the ATDs and the PMHS. While an abundance of kinematic data was obtained for each subject, this paper specifically focuses on the displacements of the 1<sup>st</sup> thoracic vertebra (T1) and bilateral acromia (Figure 4) relative to the vehicle buck coordinate system (Figure 3), which conformed to the recommendations set forth by SAE (2003). Since the PMHS subjects closely approximated the 50<sup>th</sup> percentile male, no scaling of the displacement data was performed.

### **Chest Deflection**

Chest deflection was measured by sensors mounted in the ATD thorax. The THOR SD-3 uses double-gimbaled Infrared Telescoping Rods for Assessment of Chest Compression (IR-TRACCs) to measure 3D deflection of the four quadrants of the anterior ribcage relative to the spine (Figure 2b) (Shaw et al 2012). The H3 chest included a rotary potentiometer that recorded X-axis motion of the sternum relative to the spine (chest slider) as well as string potentiometers that recorded data processed to yield X-axis and Y-axis deflection of four points on the upper and lower ribs (Butcher et al 2001) (Figure 2a). PMHS chest deflection was measured at five locations using the same motion capture system used for the kinematic measurements employing a methodology detailed in Shaw et al (2009).

### **Data Analysis and Presentation**

Comparing chest deflection involved calculating the maximum and minimum values recorded in each test and determining the mean and standard deviation for each group (PMHS, THOR SD-3, and H3). PMHS deflection data used for comparison with the dummies excluded one of the 8 subjects who had sustained 29 rib and sternal fractures. Peak deflection was calculated in two ways. The first method involved calculating an average and SD for each quadrant and, for the H3 and PMHS, the sternum. The second method involved identifying the peak X-axis motion toward the spine for each subject no matter where the deflection occurred. Because the calculation was not restricted to a specific region, the resulting average could be greater than that calculated for an individual region. For example, the location of peak deflection occurred at both the sternum and upper quadrants for the PMHS. Therefore, averaging the subjects' peak deflection at any site, either at the sternum,

upper left, or upper right, resulted in a greater “overall” peak than averaging only peak values at any one of these sites.

## RESULTS

No problems were encountered recording subject kinematics or chest deflection. The SD-3 shoulder exhibited no evidence of damage or wear in the course of the testing, and all fasteners remained snug.

### Kinematics

An overhead view of the subject kinematics in the X-Y plane of the vehicle buck is provided in Figure 5. The positions of the left acromion, right acromion, and T1 are provided for each subject at 20 ms intervals during the impact event up to the time of peak chest deflection which occurred at approximately 120 ms. Figure 5 also provides an overlay of PMHS, THOR, and H3 mean T1 and acromia positions at the time of peak chest deformation. Mean X-axis excursions for T1 and RAc are provided relative to the vehicle buck in Figure 6. Mean peak X-axis displacement values  $\pm 1$  standard deviation (SD) are provided in Figure 7.

### Chest Deflection

Figure 8 shows the average X-axis deflection time-histories for the THOR SD-3, H3, and PMHS groups. The average PMHS response is shown in thick gray lines, while the individual responses are shown as thin gray lines to illustrate subject-to-subject variability. Belt loads are also plotted in Figure 8 using the same time scale. Table 2 summarizes the peak deflection values along the positive and negative X, Y, and Z axes. For example, a negative X-axis peak indicates the closest a measurement site has moved along a perpendicular path toward the spine, while a positive X-axis peak indicates maximum motion away from the spine. Note that the H3 instruments do not record Z-axis ribcage motion. Figure 9 plots the X-axis peak values. One SD values are provided in Table 2 and indicated with error bars in Figure 9.

## DISCUSSION

### Chest Deflection

The magnitude of overall chest deflection, since it acts as a proxy for local strains in the rib cage, has been associated with thoracic injuries such as rib and sternal fractures. Specifically, a reduction in the distance between the anterior rib cage and the spine has been used as a measure of rib fracture risk (Shaw et al 2009). In frontal loading, this change in distance is approximated by the change of the X-axis component of the anterior ribcage-to-spine distance. Lateral (Y-axis) and vertical (Z-axis) motion of the anterior ribcage further characterize ribcage deformation.

Peak chest deflection, as defined by the motion of any anterior ribcage site towards the spine (negative X-axis) was found to be greatest for the PMHS. Of the dummies, the THOR SD-3 recorded a higher peak than the H3 (Figure 10).

The location of the peak X-axis deflection was different for the dummies and the PMHS. The location of the peak X-axis deflection for the dummies was always recorded at the lower left site. However, the peaks occurred for the individual PMHS at either the upper left (3/7), sternum (3/7), or the upper right measurement site (1/7). Therefore, the overall peak PMHS deflection was calculated by using peak values that occurred at three sites. Figure 11 illustrates the effect on the overall peak deflection value if the sternum is not included (“Overall Peak w/out Sternum”), a decrease of 11 percent (-66 to -59mm). Alternatively, if only the peak sternal values are used to calculate the overall average deflection, the peak is reduced by only 2 mm (-66 to -64mm). Using the H3 sternal (slider) peak value rather than the lower left reduces the overall average by only 3mm (-36 to -33mm) (Table 2).

## **Belt Path Effect on Deflection**

With one exception, the THOR SD-3 peak deflections were closer than the H3 to the average PMHS, consistent with the findings of the prior quasistatic study discussed above (Shaw et al 2005). However, both the THOR SD-3 upper right X-axis peak and the upper left/right peak ratio were less PMHS-like than the H3 (Figure 9).

The pattern of peak deflection values for the upper ribcage was related to shoulder belt position relative to the upper measurement sites. When the belt paths in the PMHS tests were examined individually, we found a robust relationship between proximity of the belt and the site of peak upper rib cage deflection (Shaw et al 2009) (Figure 12). In general, the shoulder belt path across the upper thorax in the PMHS tests generally fell between the upper left and upper right measurement sites, though there were some exceptions where the belt was lateral to the upper left measurement site. Accordingly, the PMHS upper peak values were mostly symmetrical average deflections of -48mm and -53 mm for the upper left and right, respectively. For the H3, the shoulder belt was between the upper left and right measurement sites on the ribcage, but the chest deflections were less symmetrical than the PMHS (upper right -20 mm, upper left -31 mm). For the THOR SD-3, the shoulder belt path was lateral of the upper left measurement site, and the resulting chest deflections were noticeably asymmetrical (upper right -5mm, upper left -42 mm). This asymmetry was also present in at least one individual PMHS test in which the belt path was lateral to the upper left measurement site (Figure 13). In this case the peak deflections measured at the upper chest measurement locations were almost identical between THOR SD-3 and PMHS.

In the frontal crash simulated in the reported tests, chest deflection is a function of how the inertially propelled torso loads the shoulder belt. The effects of inertial loading and the motion of the shoulder loaded by the belt were factors examined in this study.

## **Inertial Loading Effects on Deflection**

In a comparison of X-axis peak chest deflections recorded at the different measurement sites, the PMHS values generally were greater than those of the dummies (Table 2), consistent with the results for overall peak deflection and consistent with prior bench top test results for earlier versions of THOR (Shaw et al 2005). For example, a study conducted by Shaw et al (2005) compared quasistatic indenter loading of the anterior ribcage of the H3 and THOR Alpha with PMHS. For the same 25mm deflection applied to the lower quadrant, the recorded reaction force recorded by the indenter load cell was lowest for the PMHS. The reaction force for THOR Alpha was three times higher and that for the H3 thirteen times higher.

However, in this study, the lower left site for both the H3 and the THOR SD-3 moved closer to the spine (negative X-axis) than did the PMHS (Table 2, Figures 8 and 9). Assuming comparable normal belt loading, the quasistatic test results would suggest far greater PMHS deflection than either of the dummies.

The reason for this apparent incongruity may be related to differences in the loading conditions in the bench top and sled test environments. We propose that inertial loading, present in only the sled test condition, may be the most likely and dominant factor.

The possible effects of inertial loading are evident in the X-axis time history deflection plots of the lower two measurement sites (Figure 8). At approximately 50 ms the THOR SD-3 and, more prominently, the PMHS, record motion of both sites away from the spine. This motion occurs even at the lower left measurement site near the belt path. Figure 14 shows the total normal shoulder belt force relative to X-axis deflection using the method described in Salzar et al 2011. This analysis indicates that the sum of normal belt force along the belt must exceed almost 4kN before the PMHS lower left measurement site moves toward the spine (Figure 14, bottom). For the lower right measurement site farthest from the belt path, the motion away from the spine persists for both the PMHS and THOR SD-3. Neither of the H3 lower measurement sites move away from the spine, as expected since the H3 ribcage is known to be more highly coupled than that of the THOR (Shaw et al 2005).

Inertial loading acting on the anterior rib cage, as illustrated in Figure 15, is proposed as the cause for its movement away from the spine. Differential motion of the spine relative to the anterior ribcage requires a restraining force acting on the spine to resist the inertial forces pulling both the spine and anterior ribcage forward. This spine restraining force is provided by the pelvis, well restrained by the lap belt and femurs against the knee bolster, via the pelvic/spine interface. The amount of compliance in this interface and torso angle determines the amount of restraining force acting perpendicular to the upper spine.

The upper segment or segments of the dummy spine are restrained by the rubber lumbar spine. The bending stiffness of this element restrains the spine relative to the anterior ribcage during the early phase of the crash event allowing the ribcage to move away from the spine a few millimeters. This motion is limited by the low inertial forces acting on the low mass of the anterior ribcage relative to the spine box.

The PMHS thoracic spine is restrained by the lumbar spine in the same manner. However, the inertial forces acting on the anterior ribcage are not limited by the mass of the ribcage alone. The forward motion of the internal organs, not replicated in dummy thorax construction, also act to move the ribcage away from the spine. This “bulge out” is most prominent for the PMHS lower right measurement site (Figure 16). That the dummies do not replicate PMHS “bulge out” is not unexpected given a longstanding focus to replicate PMHS thoracic response to compressive loading.

### **Shoulder Motion**

The motion of the loaded shoulder and clavicle is both a response and determinant of shoulder belt interaction with the torso. The normal belt load born by the torso is shared by the clavicle/shoulder complex and the anterior rib cage (Horsch et al 1991). The farther forward the shoulder moves, the more the belt is loaded by the shoulder and the less it is loaded by the anterior ribcage resulting in lower chest deflection.

Figure 5 illustrates differences in the kinematic behavior between PMHS and the ATDs. When viewed from above, the PMHS exhibit a greater clockwise rotation of the shoulders about the vertical Z-axis of the vehicle buck than either of the ATDs. This is most apparent when looking at the overlay of all subjects at 120 ms (Figure 5), which is also the approximate time of peak chest deflection. Relative to the H3, the PMHS are considerably more rotated, however, the comparison with THOR is more complex. The line segment connecting the left acromion (LAc) and T1 are very similarly angled for THOR and the PMHS; however this trend is not repeated for the loaded right shoulder. The line connecting the right acromion (RAc) and T1 is angled much more forward for THOR than for the PMHS, or even the H3.

The PMHS exhibit the largest forward excursion of T1 and also the largest difference between the RAc and T1 excursions relative to the vehicle buck (Figures 6 and 7). THOR exhibits nearly equal excursions of both RAc and T1.

Although this analysis found substantial differences among the test subjects, a more sophisticated analysis is required to fully characterize shoulder and torso motion and to quantify upper spine rotation and its potential effect on chest deflection.

### **Limitations**

This study was not intended to be a definitive evaluation of dummy performance in terms of its ability to approximate the response of PMHS in a frontal crash. The scope of the study was limited to one of at least three test conditions proposed by UVA for the Gold Standard simulated frontal impacts, an effort to produce PMHS-derived performance targets. Findings such as the bulge out may not be as prominent in conditions that do not block the knees at the start of the event. The proposed reason for the bulge out, inertial loading, while consistent with the study findings, was not quantified.

The locations of anterior ribcage measurement sites for the three subjects are in the same quadrant but not necessarily the same location within the quadrant (Figure 2). Although the ribcage deflection measurements

sites on the PMHS targeted similar locations on THOR, constraints in instrument mounting compromised the final location for some subjects. The H3 sites, especially the upper sites, are in different locations relative to THOR and the PMHS.

Study limitations prevent definitive conclusions regarding shoulder motion and its effect on chest deflection. Clavicle motion was estimated by the motion of a segment connecting the T1 and the acromion. However, the motion of the clavicle itself, likely the shoulder component most loaded by the belt, was not measured directly. While the distal end of the clavicle moves with the acromion, the medial end joins the top of the sternum which moves with the (deforming) ribcage. Another parameter not adequately quantified was the position of the belt relative to the clavicle throughout the event. A belt that loaded the clavicle near the sternum would be less affected by forward motion of the distal clavicle/acromion.

The tested THOR SD-3 was a pre-production prototype constructed from a combination of used and new components.

## **CONCLUSIONS AND RECOMMENDATIONS FOR FURTHER STUDY**

The THOR SD-3 sustained no damage or sensor failures during the course of the nine-test series. While not a comprehensive assessment of durability, this result is encouraging.

In general, THOR SD-3 peak X-axis chest deflection values for the anterior measurement sites were closer to those of the PMHS than the H3 (Figure 9). However, the deflection response of neither dummy approached that of the PMHS relative to motion of the anterior ribcage away from the spine (positive X-axis). Further investigation is needed to define the effects of inertial loading, motion of the anterior ribcage away from the spine, and, most importantly, its effect on fracture risk.

The THOR SD-3 also exhibited a PMHS-like deflection sensitivity to belt position, a characteristic reported for the H3. Fully characterizing sensitivity to belt position may produce a valuable dummy response performance target. Additional work would be needed to relate this parameter to fracture risk.

The PMHS rearward motion of the loaded shoulder may result in increased chest deflection, while the forward motion of the THOR SD-3 may limit chest deflection. The H3 loaded shoulder motion was likely limited by the stiff H3 shoulder design and limited range of motion. Because the shoulder interaction with the belt is a determinant of chest deflection, further study of the THOR SD-3 shoulder belt interaction is suggested. Similarly a comprehensive study of spinal kinematics with focus on spinal rotations that may substantially influence interaction between the ribcage and the shoulder belt is also warranted.

## **ACKNOWLEDGMENTS**

The authors acknowledge the support and guidance of the National Highway Traffic Safety Administration (NHTSA), U S Department of Transportation. This study was supported by DOT NHTSA Grant DTNH22-09-H-00247. All findings and views reported in this manuscript are based on the opinions of the authors and do not necessarily represent the consensus or views of the funding organization.

## **REFERENCES**

- Allsop, D, Kennett, K. Skull and Facial Bone Trauma. in *Accidental Injury: Biomechanics and Prevention- 2nd Edition*, editors, Nahum AM;Melvin J. 2002; New York: Springer.
- Backaitis, S, Dalmotas, D. Injury Patterns and Injury Sources of Unrestrained and Three Point Belt Restrained Car Occupants in Injury Producing Frontal Collisions. *Proceedings of the Association for the Advancement of Automotive Medicine (AAAM)*. 1985;29.
- Bostrom, O, Haland, Y. Benefits of a 3+2 point belt system and an inboard torso side support in frontal, far-side and rollover crashes. Paper 451, *International Technical Conference on the Enhanced Safety of Vehicles (ESV)*. 2003; 18. Nagoya,Japan.
- Butcher, J, Shaw, CG, Bass, CR, Kent, RW, Crandall, JR. Displacement Measurements in the Hybrid III Chest. *SAE Transactions: Journal of Passenger Cars*. 2001;110(6): 26-31. Based on SAE Paper 2001-01-0118.
- Elvik R, Vaa, T. *The handbook of road safety measures*. 2004;Amsterdam, Elsevier Science.
- Foret-Bruno, J, Le Cox, J, Thomas, C, Brutel, G. In Depth Analysis of Frontal Collisions As Regards the Influence of Overlap and Intrusion On Occupant Severe and Fatal Injuries. *International Technical Conference on the Enhanced Safety of Vehicles (ESV)*. 1994;14.
- Forman, JL, Lessley, DJ, Kent, RW, Bostrom, O, Pipkorn, B. Whole-body Kinematic and Dynamic Response of Restrained PMHS in Frontal Sled Tests. *Stapp Car Crash Journal*. 2006;50: 299-336.
- Horsch, J, Melvin, J, Viano, DC, Mertz, H. Thoracic injury assessment of belt restraint systems based on Hybrid III chest compression. Paper 912895, *Society of Automotive Engineers*. 1991.
- Huelke, DF, Sherman, HW, Murphy, MJ, Kaplan, RJ. Effectiveness of Current and Future Restraint Systems in Fatal and Serious Injury Automobile Crashes. Data From On-Scene Field Accident Investigations. Paper 790323, *Society of Automotive Engineers (SAE)*. 1979.
- Kent, RW, Balandin, D, Bolotnik, N, Pilkey, WD, Purtsezov, S. Optimal control of restraint forces in an automobile impact. *Journal of Dynamic Systems, Measurement, and Control*. 2007;129: 415-424.
- Lemmen, P, Bernard Been Jolyon Carroll, David Hynd Johan Davidsson Jeff Crandall, Greg Shaw Cecilia Sunnevang Autoliv Research Erwan Lecuyer, Eric Song Andre Eggers Luis Martinez Philippe Vezin. (2013) *An Advanced Thorax-Shoulder Design for the THOR Dummy*. Submitted to 2013 ESV.
- Lessley, DJ, Shaw, CG, Riley PO, Forman, JL, Crandall, JR. Assessment and Validation of a Methodology for Measuring Anatomical Kinematics of Restrained Occupants During Motor Vehicle Collisions. *Journal of Biosensors and Bioelectronics*. 2011;S1.
- Morris, A, Welsh, R, Frampton, R, Charlton, J, Fildes, B. An Overview of Requirements for the Crash Protection of Older Drivers. *Annual Proceedings/Association for the Advancement of Automotive Medicine (AAAM)*. 2002;46:141-156.
- Morris, A, Welsh, R, Hassan, A. Requirements for the Crash Protection of Older Vehicle Passengers. *Annual Proceedings/Association for the Advancement of Automotive Medicine (AAAM)*. 2003;47:165-180.
- NHTSA. *Motor vehicle occupant protection facts 2006*. 2008;Washington, DC, National Highway Traffic Safety Administration.
- NHTSA. *Fatalities in Frontal Crashes Despite Seat Belts and Air Bags. Review of All CDS Cases Model and Calendar Years 2000-2007 122 Fatalities*. 2009;HS 811 202, September, NHTSA US DOT, Washington, DC.
- Parent, DP, Lessley, DJ, Shaw, CG, Crandall, JR. Identification of anatomical landmarks for whole-body kinematic measurement in the THOR Mod Kit frontal impact ATD. Paper 20125177, *JSAE Annual Congress*. 2012.

- Ridella, SA, Parent, DP. Modifications to Improve the Durability, Usability and Biofidelity of the THOR-NT Dummy. Paper Number 11-0312. Proceedings of the 22nd International Conference on the Enhanced Safety of Vehicles (ESV). 2011
- Rouhana SW; Bedewi PG; Kankanala SV; Prasad P; Zwolinski JJ; Medovsky AG; Rupp JD; Jeffreys TA; Schneider LW. Biomechanics of 4-Point Seat Belt Systems in Frontal Impacts. Stapp Car Crash Journal. 2003;47: 367-399.
- Salzar, RS, Lessley, DJ, Sochor, MR, Shaw, CG, Kent, RW, Crandall, JR. Thoracic Response to Shoulder-Belt Loading: Comparison of Table-Top and Frontal Sled Tests with PMHS. IRCOBI Conference on the Biomechanics of Impact. 2011.
- Shaw, CG, Lessley, DJ, Ash, JH, Crandall, JR. Development of an Alternative Frontal Impact Condition to Assess Thoracic Response Using the THOR Mod Kit Dummy. 2012;Paper 20125216, JSAE Annual Congress.
- Shaw, CG, Lessley, DJ, Kent, RW, Crandall, JR. Dummy Torso Response to Anterior Quasi-Static Loading. Paper 05-0371, Proceedings of the 19th International Technical Conference on the Enhanced Safety of Vehicles (ESV). 2005.
- Shaw, CG, Parent, D, Purtsezov, S, Lessley, D, Crandall, JR, Kent, RW, Guillemot, H, Ridella, SA, Takhounts, E, Martin, P. Impact response of restrained PMHS in frontal sled tests: skeletal deformation patterns under seat belt loading. Stapp Car Crash Journal. 2009;53:1-48.
- Shaw, CG, Parent, DP, Purtsezov, S, Lessley, DJ, Crandall, JR, Tornvall, F. (2010) Torso deformation in frontal sled tests: comparisons between THOR NT, THOR NT with Chalmers SD-1 shoulder, and PMHS. IRCOBI Conference on the Biomechanics of Impact.
- Society of Automotive Engineers. Surface Vehicle Recommended Practice J211-1 –Instrumentation for Impact Test – Part 1 –Electronic Instrumentation, Warrendale, PA. 2003
- Viano DC; Melvin JW; McCleary JD; Madeira RG; Shee TR; Horsch JD. Measurement of Head Dynamics and Facial Contact Forces in the Hybrid III Dummy. Paper 861891. Stapp Car Crash Conference Proceedings. 1986.
- Viano, D, Ridella, S. Crash Causation: a Case Study of Fatal Accident Circumstances and Configurations. Paper 960458, Society of Automotive Engineers (SAE). 1996.

## Figures

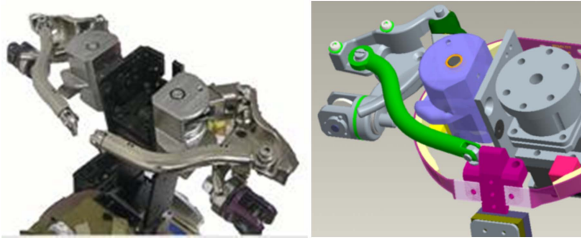
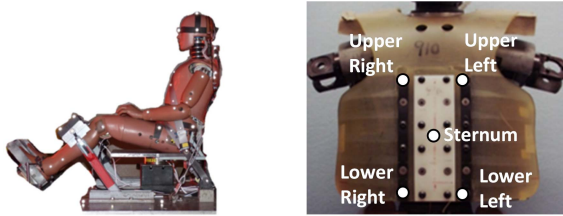
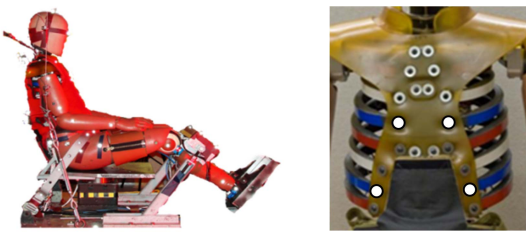


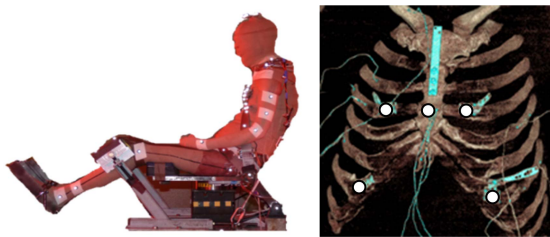
**Figure 1.** SD-3 shoulder.



a Hybrid III

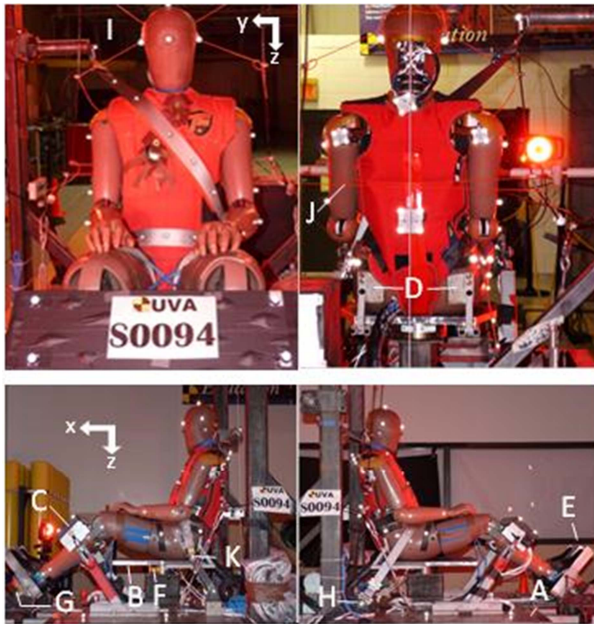


b THOR SD-3



c PMHS

**Figure 2.** Study subjects and location of deflection measurement sites on the anterior ribcage.



A	Buck	Restraint geometry similar to 1998 Ford Taurus front passenger position.
B	Seat	Rigid horizontal aluminum plate.
C	Knee bolster	Adjustable bilateral non-padded knee channels atop 5-axis load cells.
D	Pelvic block	Adjustable bilateral blocks to prevent pelvic posterior migration pre-test.
E	Footrest	Adjustable bilateral channels with ankle straps to immobilize feet and lower legs.
F	Seat load cell	6-axis load cell supporting seat.
G	Footrest load cell	6-axis load cell supporting seat.
H	Right lap belt anchor	Center of bolt head securing the right belt to the anchor mount defines the buck coordinate system for 3D movement data. Lap belt length adjuster tongue mounts here.
I	Upper shoulder belt anchor	Center of bolt head securing upper shoulder belt segment. Adjustable in Z and Y.
J	Back	Adjustable back and head support provided by horizontal wires attached to vertical cables.
K	Left lap and shoulder belt anchor	Anchor point is position at an OEM location by a "stalk" surrogate. Shoulder belt length adjuster tongue and the left lap belt anchor mount here.

**Figure 3.** Test hardware. Thor SD-3 shown.

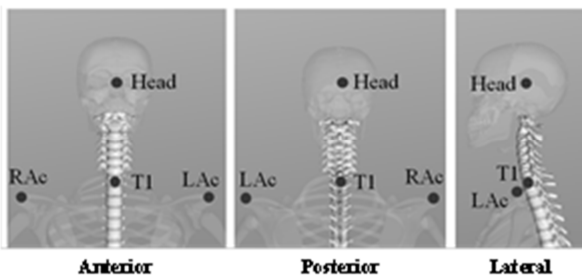


**Figure 4.** Calculated anatomical kinematic measurement locations.

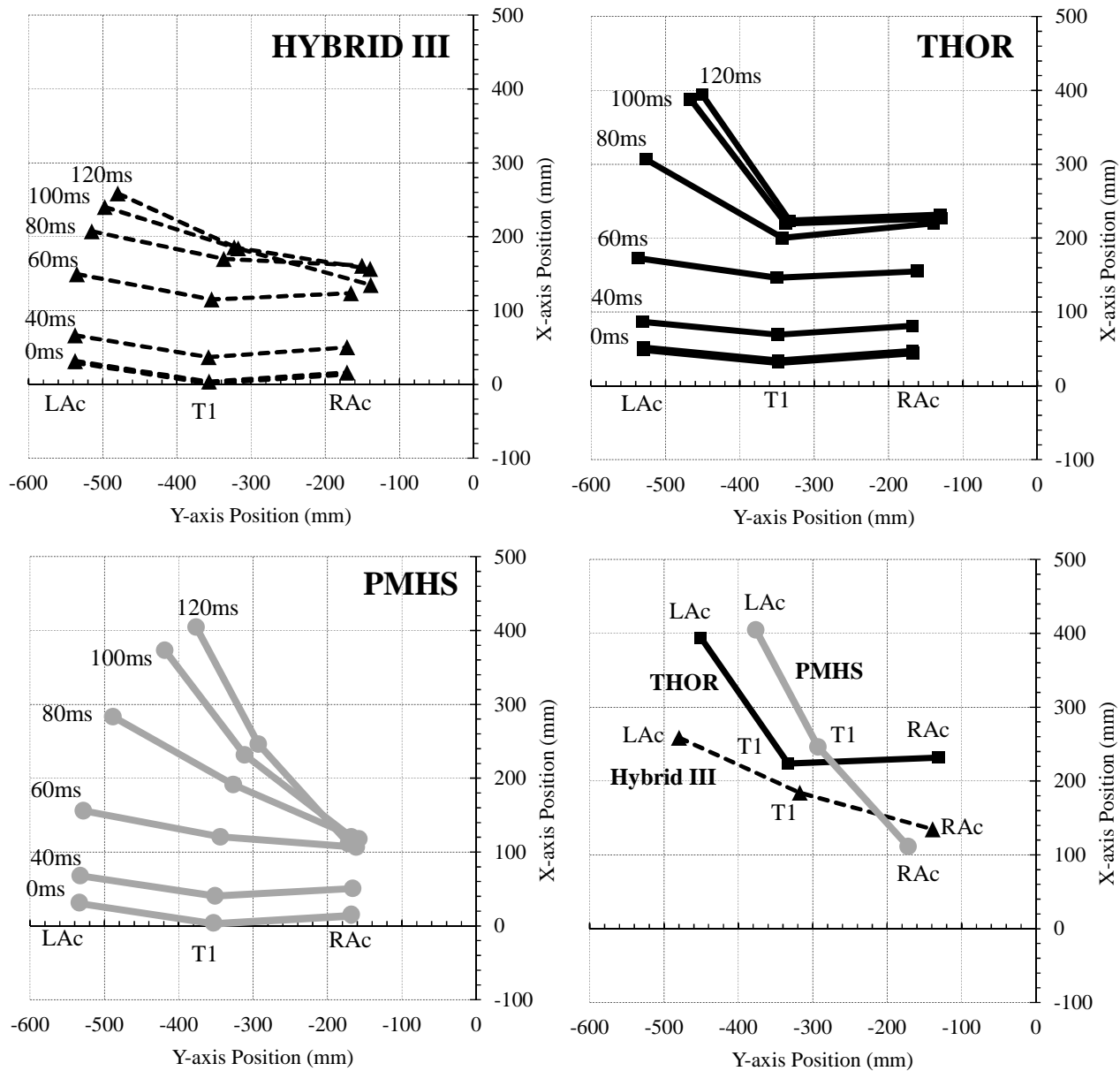


**Figure 5.** Overhead view of subject kinematics. Position of T1 and bilateral acromia at 20 ms intervals for each subject. Overlay of all subjects at 120 ms (lower right plot).

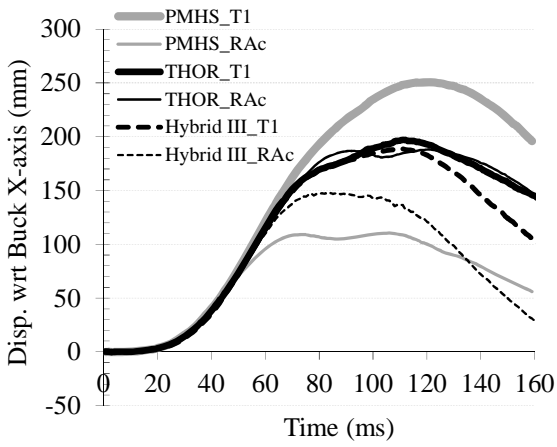


**Figure 6.** Right Acromion (RAc) and T1 displacement with respect to the vehicle buck. Plots represent the mean from all available tests for each subject.

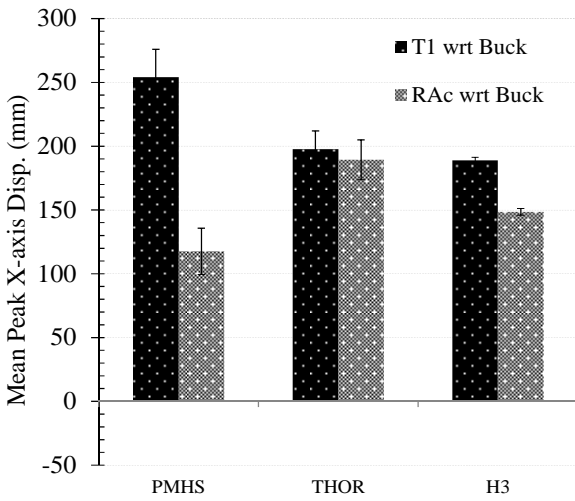


**Figure 7.** Mean Peak X-axis displacements  $\pm$  1 S.D. for each subject.

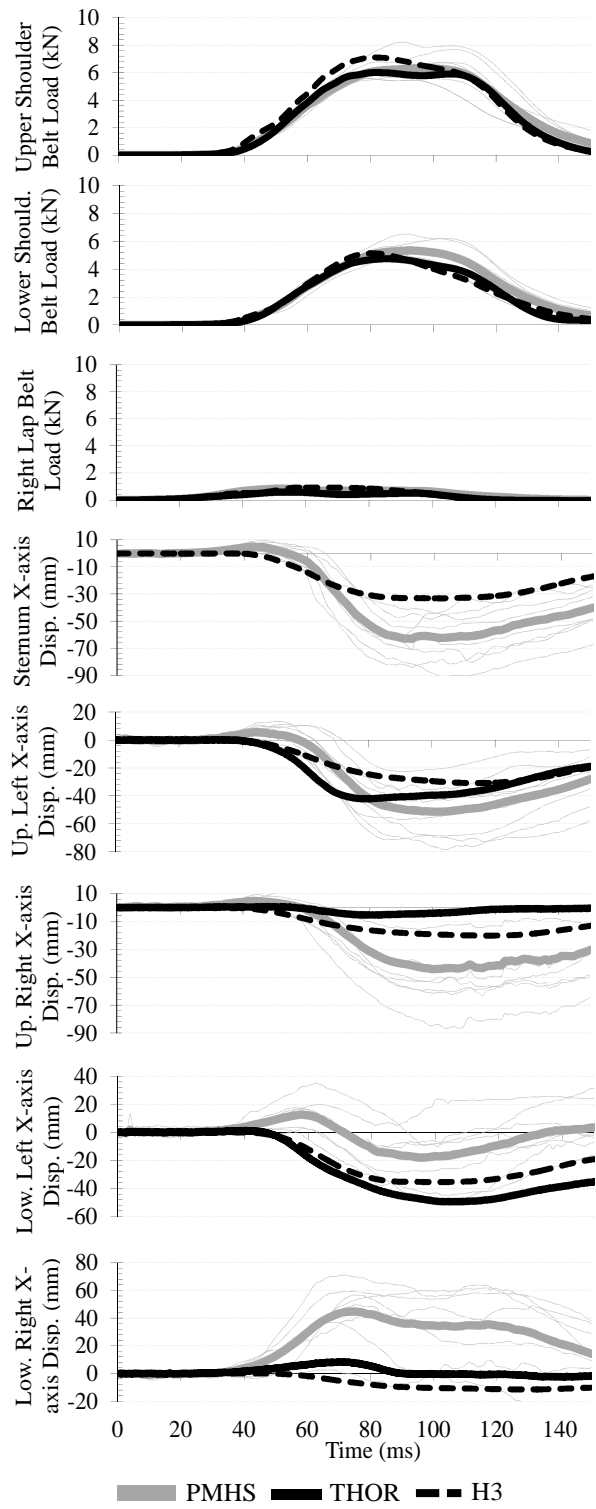


**Figure 8.** X-axis chest deflection, sled pulse, and belt loads.

**Table 2.** GS1 Chest Deflection.

		Upper Right						Sternum						Upper Left					
		+X	-X	+Y	-Y	+Z	-Z	+X	-X	+Y	-Y	+Z	-Z	+X	-X	+Y	-Y	+Z	-Z
<b>H3</b>	mm	0	<b>-20</b>	7	-1			0	<b>-33</b>					0	<b>-31</b>	4	-1		
	SD	0	0	1	0			0	0					0	0	1	0		
<b>HOR SD-3</b>	mm	<b>1</b>	-5	<b>11</b>	<b>-8</b>	6	-14							<b>1</b>	<b>-42</b>	<b>10</b>	<b>-5</b>	17	-7
	SD	0	1	1	1	1	1							0	1	2	1	1	1
<b>PMHS</b>	mm	11	-48	32	-6	16	-20	9	-67	27	-14	21	-10	9	-53	34	-5	15	-11
	SD	10	27	3	7	8	17	5	18	7	11	7	9	6	20	6	6	9	9
		Lower Right						Lower Left											
		+X	-X	+Y	-Y	+Z	-Z	+X	-X	+Y	-Y	+Z	-Z						
<b>H3</b>	mm	0	<b>-12</b>	6	-1									0	<b>-36</b>	3	-4		
	SD	0	0	1	1			Bold indicates value closer to PMHS						0	1	1	1		
<b>HOR SD-3</b>	mm	<b>9</b>	-3	<b>11</b>	<b>-6</b>	10	-6							<b>4</b>	-50	<b>19</b>	-4	11	-10
	SD	1	1	1	2	0	1							1	2	1	3	0	0
<b>PMHS</b>	mm	49	-7	43	-2	13	-53							16	-22	45	-2	13	-33
	SD	19	12	10	1	7	21							13	18	14	1	4	11

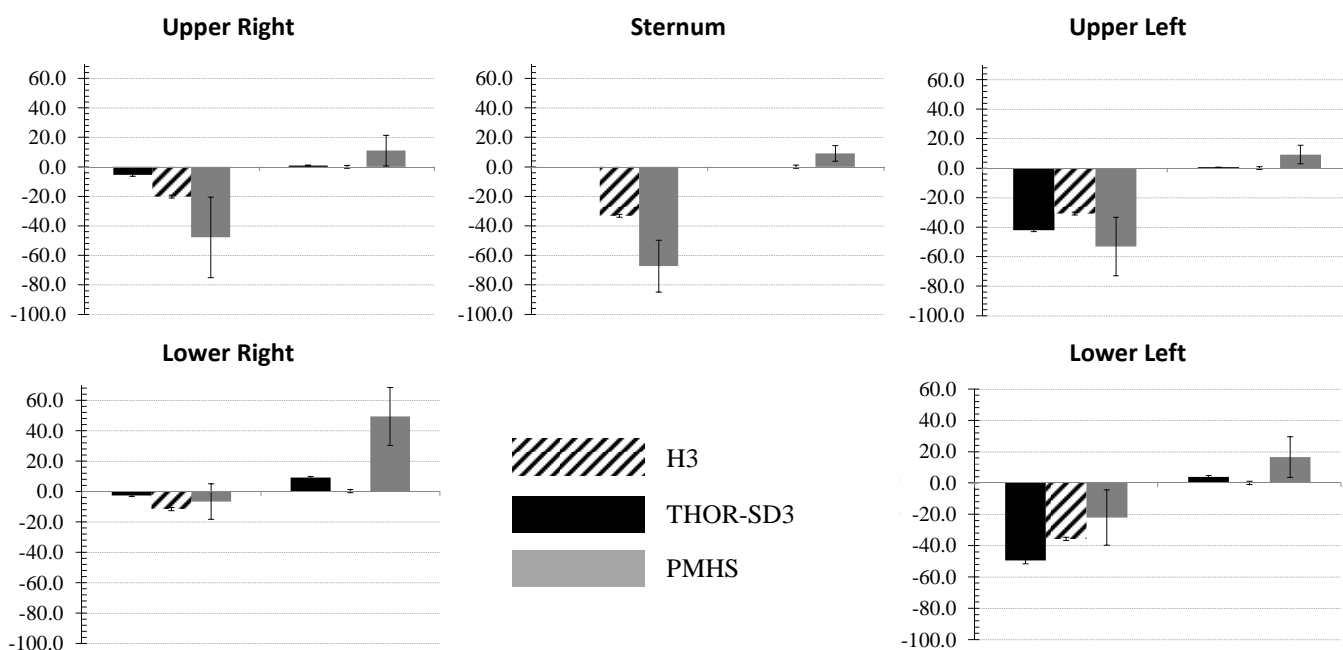


**Figure 9.** GS1 X-axis deflection. Average values with 1 SD.

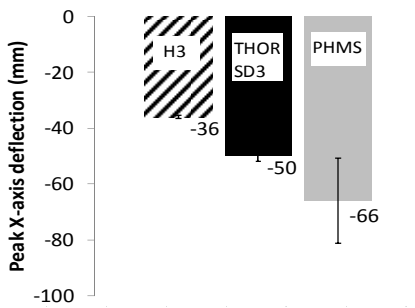


**Figure 10.** Peak X-axis deflection (with standard deviation) towards the spine, any site.

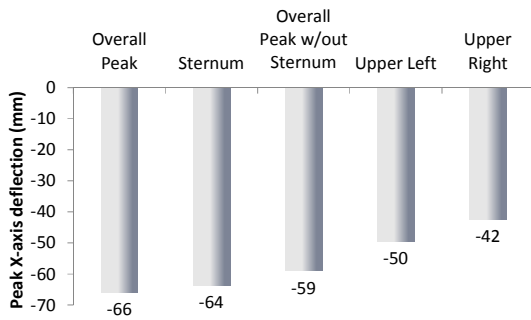


**Figure 11.** PMHS average X-axis peak deflections for the sternum and upper measurement sites.

Overall Peak	Average of peak values where ever they occur
Sternum	Average of sternal peak values only
Overall Peak w/out Sternum	Average of peak values where ever they occur excluding the sternum
Upper Left	Average of upper left peak values only
Upper Right	Average of upper right peak values only

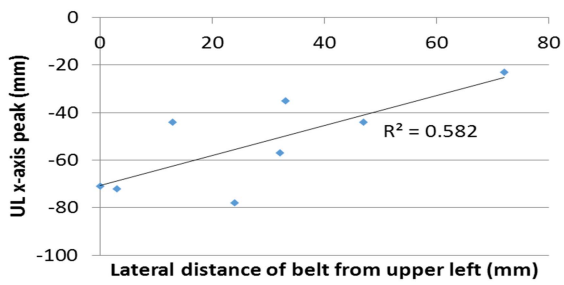
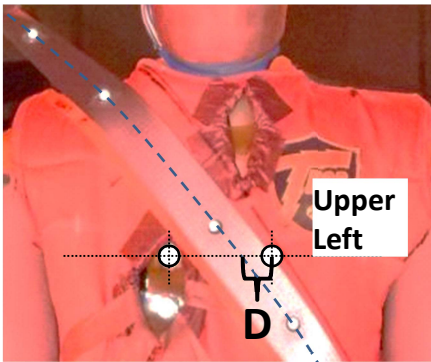
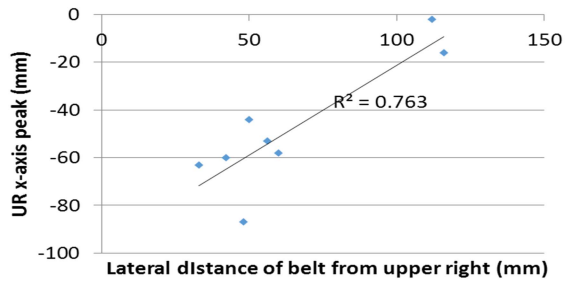
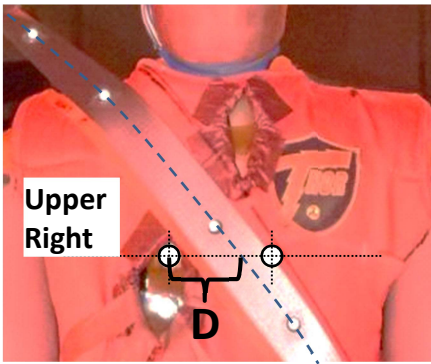


**Figure 12** . Relationship between measurement site distance to belt path and peak deflection.

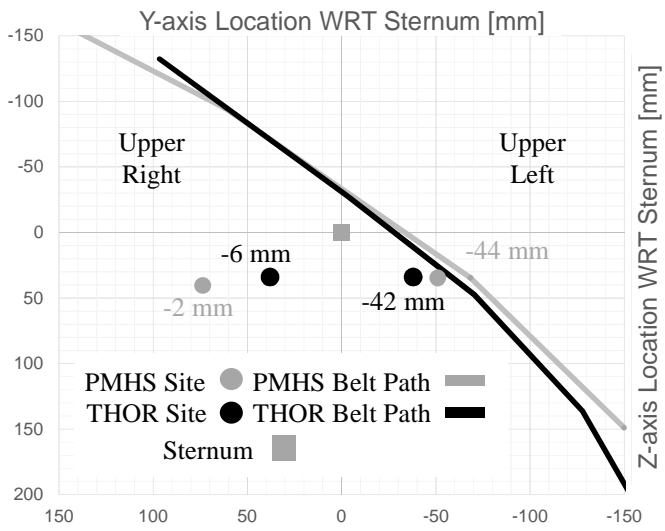


**Figure 13.** Belt paths, upper measurement sites, and X-axis deflections of a single PMHS and THOR.

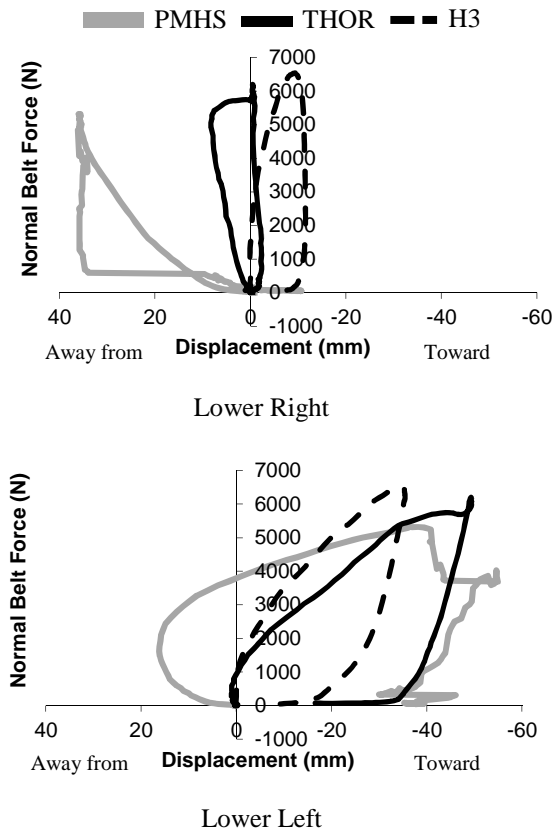


**Figure 14.** Total normal shoulder belt force relative to X-axis displacement.

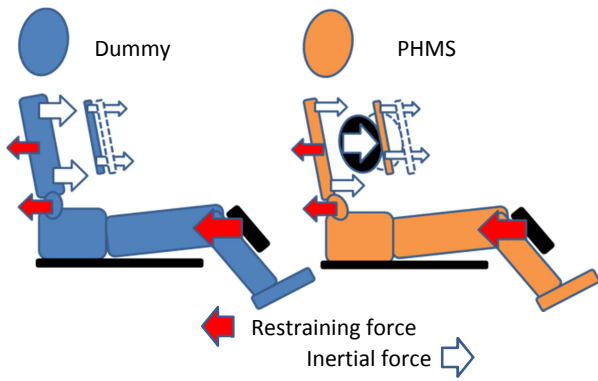


**Figure 15.** Forces acting to move anterior ribcage away from the spine.

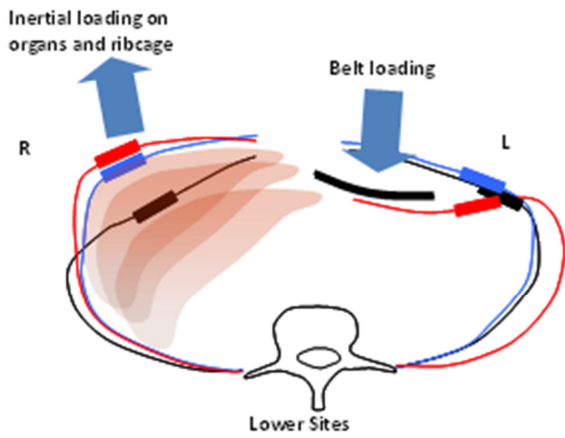


**Figure 16.** Bulge out for the lower right PMHS measurement site.